Proceedings of the 7th International Workshop on Human-friendly Welfare Robotic Systems, 22-24 October 2006

Robustifying Internal Model Control

Gun Rae Cho, Pyung Hun Chang, and Sang Hyun Park
Department of Mechanical Engineering
Korea Advanced Institute of Science and Technology
373-1 Guseong-dong, Daejeon 305-701, Korea
E-mail : {blueid, phchang, hyunmu}@kaist.ac.kr

Abstract

The robustness problem in the time delay control (TDC) against the discontinuous dynamics of robot manipulators, such as Coulomb friction, is revealed in this paper. As a remedy for this problem, an enhanced controller is proposed and its properties and stability are analyzed. The proposed controller has a compensator based on the internal model control (IMC) concept. It is effective in handling the adverse effects of friction; moreover, it is simple and efficient and becomes a positive attribute of TDC. The controller does not need the entire plant model and thus, it can be applied easily. The simulation and experimental results show the effectiveness of the proposed controller.

1. Introduction

This paper presents an enhanced controller which improves the robustness of the time delay control (TDC) against the discontinuous dynamics of robot manipulators, such as Coulomb friction, by using the internal model control (IMC) concept. The background and context for this research is provided below.

The TDC [1,2] is a control technique that estimates and compensates system uncertainties, such as unmodeled dynamics, parameter variations, and disturbances, by utilizing a time-delayed signal of certain system variables. Owing to the effectiveness and efficiency of the time delay estimation (TDE), the TDC has an unusually compact structure and relatively simple gain selection procedure. After research on the TDC was firstly reported, the TDC has been applied to many mechanical, electric, and electromechanical systems. Particularly, the TDC exhibits a good performance when controlling robot manipulators. Hsia *et al.* have applied the TDC to problems of position control, force control, and impedance control for robot manipulators and have obtained good results [3-5]. Chang *et al*. have applied the TDC to the problem of hybrid position/force control for robot manipulators and they showed that the TDC exhibited robust responses [6,7]. Also, the experimental results of well-known heavy duty systems, such as robotic excavators and telescopic handlers, showed that the TDC is a simple and robust control scheme [8,9].

It has been observed, however, that the TDC reveals some problems in the presence of discontinuous dynamics. For example, Coulomb friction increases the tracking error when a plant passes by zero velocity and degrades the transient response of the controlled system. As will be explained in Section II, these phenomena of the TDC come from the TDE error. The TDE treats that the plant dynamics of a previous sampling time is similar to that of the current sampling time, and it is valid under the assumption that the plant dynamics varies continuously. However, in the presence of discontinuity (or very fast dynamics) in the plant dynamics, this assumption is invalid so the accuracy of the TDE degrades. Accordingly, the controlled system has a large tracking error.

Coulomb friction dynamics, one of the major contributing factors of discontinuity, is an important aspect for industrial robot manipulators. For example, Coulomb friction levels as high as 30 percent of the maximum motor torque is not uncommon in some industrial robot manipulator drive trains, such as a PUMA arm [10]. Furthermore, [11] showed the significance of Coulomb friction with case studies of micro and macro manipulators and also reported that friction can cause 50 percent error in some heavy industrial manipulators.

There is a little research on improving the robustness of the TDC. The main part of this research presents a remedy by adopting the sliding mode control (SMC) and shows its effectiveness by applying it to an excavator system [12], pneumatic cylinder system [13], and DC servo motor [14]; however, it has some drawbacks. Occasionally, its inherent use of discontinuous input causes chattering in the tracking response. In addition, it needs extra gain tuning for compensators, which can be a burden in the design procedures of controllers. Besides this, an enhanced perturbation observer was proposed in [15]. This has some multi-loop stages of a perturbation observer that are known to use a similar algorithm as the TDC.

In this paper, a compensator is proposed to improve the robustness of the TDC against discontinuous dynamics, such as Coulomb friction. The proposed compensator is designed based on the concept of the IMC. The IMC is the control algorithm that uses the plant model directly [16,17]; it has a straight forward design method and good control performance to provide a theoretically perfect control scheme. It has also been widely used to control chemical processes [18,19] and robot manipulators by adding the

computed torque control [20]. After all, an enhanced controller, called the time delay control with internal model (TDCIM), that combines the two concepts of TDC and IMC is proposed to handle the discontinuous friction dynamics of robot manipulators.

This paper is organized as follows. In Section II, the problems of the TDC are analyzed and the IMC is reviewed briefly. In Section III, the enhanced controller is proposed and its properties are analyzed. The robustness of proposed controller is verified with the simulation and experimental results in Section IV. Finally, the results are summarized and conclusions are drawn in Section V.

2. Problems of the TDC and review of the IMC

In order to point out its problems, the TDC is briefly reviewed and analyzed with simulation results. Also, the IMC is introduced; it is adopted to handle the problems of the TDC.

2.1 Problems of the TDC

We summarize the TDC law for robot manipulators [2] and analyze its problems concerning TDE error.

2.1.1 Review of the TDC

The dynamics of *n* DOF robot manipulators is generally described as follows:

$$\mathbf{M}(\boldsymbol{\theta})\ddot{\boldsymbol{\theta}} + \mathbf{V}(\boldsymbol{\theta},\dot{\boldsymbol{\theta}}) + \mathbf{G}(\boldsymbol{\theta}) + \mathbf{F}(\boldsymbol{\theta},\dot{\boldsymbol{\theta}}) = \boldsymbol{\tau}, \quad (1)$$

where $\boldsymbol{\theta},\dot{\boldsymbol{\theta}},\ddot{\boldsymbol{\theta}} \in \Re^n$ denote the joint angle, joint angular velocity, and joint angular acceleration, respectively; $\mathbf{M}(\boldsymbol{\theta}) \in \Re^{n\times n}$ denotes the inertia matrix; $\mathbf{V}(\boldsymbol{\theta},\dot{\boldsymbol{\theta}}) \in \Re^n$ denotes the Coriolis and the centrifugal forces; $\mathbf{G}(\boldsymbol{\theta}) \in \Re^n$ denotes gravity; $\mathbf{F} \in \Re^n$ denotes frictions and unmodeled disturbances; and $\boldsymbol{\tau} \in \Re^n$ denotes the input torque.

By importing the constant matrix $\bar{\mathbf{M}} \in \Re^{n\times n}$, which represents the known range of **M,** (1) can be rewritten as follows:

$$\bar{\mathbf{M}}\ddot{\boldsymbol{\theta}} + \mathbf{H}(\boldsymbol{\theta},\dot{\boldsymbol{\theta}},\ddot{\boldsymbol{\theta}}) = \boldsymbol{\tau}, \quad (2)$$

where **H** denotes the total sum of the nonlinear dynamics of robot manipulators and is described as follows:

$$\mathbf{H}(\boldsymbol{\theta},\dot{\boldsymbol{\theta}},\ddot{\boldsymbol{\theta}}) = (\mathbf{M}(\boldsymbol{\theta}) - \bar{\mathbf{M}})\ddot{\boldsymbol{\theta}} + \mathbf{V}(\boldsymbol{\theta},\dot{\boldsymbol{\theta}}) + \mathbf{G}(\boldsymbol{\theta}) + \mathbf{F}(\boldsymbol{\theta},\dot{\boldsymbol{\theta}}). \quad (3)$$

Generally, $\boldsymbol{\tau}$ can be designed based on the computed torque control as follows:

$$\boldsymbol{\tau} = \bar{\mathbf{M}}\mathbf{u} + \hat{\mathbf{H}}, \text{ and} \quad (4)$$

$$\mathbf{u} = \ddot{\boldsymbol{\theta}}_d + \mathbf{K}_D\left(\dot{\boldsymbol{\theta}}_d - \dot{\boldsymbol{\theta}}\right) + \mathbf{K}_P\left(\boldsymbol{\theta}_d - \boldsymbol{\theta}\right), \quad (5)$$

where $\hat{\mathbf{H}}$ denotes the estimated value of **H**; $\boldsymbol{\theta}_d,\dot{\boldsymbol{\theta}}_d,\ddot{\boldsymbol{\theta}}_d \in \Re^n$ denotes the desired trajectory; and $\mathbf{K}_D \in \Re^{n\times n}$ and $\mathbf{K}_P \in \Re^{n\times n}$ represent the PD gain diagonal matrices.

When implementing the controller, it is very important to estimate **H** precisely, because the control performance depends directly on the accuracy of the estimation of **H**. The control objective is to cause the closed loop system to have the desired error dynamics described below by estimating **H** exactly, i.e. $\hat{\mathbf{H}} = \mathbf{H}$ in an ideal case.

$$\ddot{\mathbf{e}} + \mathbf{K}_D\dot{\mathbf{e}} + \mathbf{K}_P\mathbf{e} = \mathbf{0}, \quad (6)$$

where $\mathbf{e} \equiv \boldsymbol{\theta}_d - \boldsymbol{\theta}$.

The TDC uses the time delay estimation (TDE) to obtain $\hat{\mathbf{H}}$. Under the assumption that the time delay *L* is sufficiently small, the following approximation is valid from (2):

$$\mathbf{H}_{(t)} \cong \hat{\mathbf{H}}_{(t)} = \mathbf{H}_{(t-L)} = \boldsymbol{\tau}_{(t-L)} - \bar{\mathbf{M}}\ddot{\boldsymbol{\theta}}_{(t-L)}. \quad (7)$$

Finally, the TDC is expressed as:

$$\boldsymbol{\tau} = \boldsymbol{\tau}_{(t-L)} - \bar{\mathbf{M}}\ddot{\boldsymbol{\theta}}_{(t-L)} + \bar{\mathbf{M}}\left[\ddot{\boldsymbol{\theta}}_d + \mathbf{K}_D\left(\dot{\boldsymbol{\theta}}_d - \dot{\boldsymbol{\theta}}\right) + \mathbf{K}_P\left(\boldsymbol{\theta}_d - \boldsymbol{\theta}\right)\right]. \quad (8)$$

If $\bar{\mathbf{M}}$ is selected as the diagonal constant matrix, the TDC can be designed as separate joint controller using only $\bar{\mathbf{M}}$ and PD gains, as in Fig. 1. Thus, the TDC is very simple and efficient and has few computation burdens because of using the TDE, which does not need to compute the entire robot manipulator dynamics.

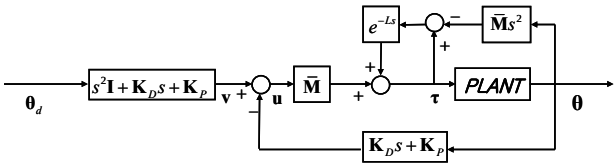

Fig. 1. Block diagram of the TDC

2.1.2 Problems of the TDC concerned with the TDE error

If the time delay *L* is set infinitesimally small, it is possible to estimate **H** precisely using the TDE. Because of hardware limitations, however, *L* must be set for a finite time interval. Generally, controllers are implemented with digital devices, and the smallest value for the time delay *L* is the sampling time, which is finite. Therefore, the TDE error exists due to a finite *L*. From (2), (4), and (7), the following is derived:

$$\bar{\mathbf{M}}\left(\mathbf{u}_{(t)} - \ddot{\boldsymbol{\theta}}_{(t)}\right) = \mathbf{H}_{(t)} - \hat{\mathbf{H}}_{(t)} = \mathbf{H}_{(t)} - \mathbf{H}_{(t-L)}. \quad (9)$$

The right side term of the above equation denotes the TDE error. Here, the TDE error is defined as:

$$\boldsymbol{\varepsilon}_{(t)} \equiv \mathbf{u}_{(t)} - \ddot{\boldsymbol{\theta}}_{(t)} = \bar{\mathbf{M}}^{-1}\left(\mathbf{H}_{(t)} - \mathbf{H}_{(t-L)}\right). \quad (10)$$

The error dynamics of the TDC is represented as follows and it shows the influence of the TDE error on the tracking error:

$$\ddot{\mathbf{e}}_{(t)} + \mathbf{K}_D\dot{\mathbf{e}}_{(t)} + \mathbf{K}_P\mathbf{e}_{(t)} = \boldsymbol{\varepsilon}_{(t)}. \quad (11)$$

The effectiveness of the TDE determines the robustness of the closed loop system against the plant nonlinearity and disturbances. Closely related to the effectiveness of the TDE, the value of the time delay *L* is a crucial factor. Qualitatively speaking, the time delay *L* needs to be selected so that the

continuity assumption of $\mathbf{H}_{(t)}$ is valid. In mechanical systems, however, discontinuous (or very fast) dynamics, such as the Coulomb frictions, exists and cannot be estimated accurately using the TDE with a finite L. Therefore, when the TDC is applied to such systems, the TDE error increases resulting in a large tracking error occurs.

2.1.3 Simulation under Coulomb friction

To observe the problem of the TDC due to the TDE error more clearly, the TDC is analyzed using simulation results under Coulomb friction dynamics. A 1 DOF link system, as described in Fig. 2, is used in this simulation and gravity is not considered. This plant has nonlinear dynamics due only to friction, so it is an appropriate plant for observing the properties of the controller against the friction effect.

Generally, coulomb friction is modeled as follows.

$$F = \tau_{slip}\,\mathrm{sgn}\left(\dot{\theta}\right) \qquad (12)$$

where, τ_{slip} denotes coulomb friction coefficient. When plant goes across zero velocity, coulomb friction changes its direction and plant has discontinuous dynamics. And this effect degrades control performance in tracking control.

In this simulation, the TDC with $\bar{M} = 1.0$ is applied to the plant with the friction as described above. The PD gains are fixed at K_D=20 and K_P=100 to cause the error dynamics in (11) to have a natural frequency of ω_n=10 rad/sec with critical damping. To observe the Coulomb friction effect in the tracking control, the reference velocity is set to increase linearly and to cross zero velocity at t=1 sec.

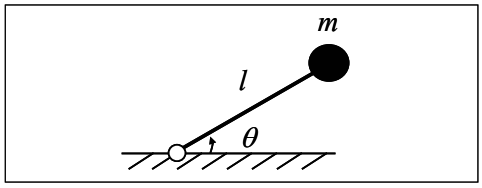

Fig. 2. 1 DOF link system. $l = 1.0(m)$ and $m = 1.0(kg)$

The simulation results are shown in Fig. 3: (a) is the conceptual figure of the estimation error of **H** and (b) is the tracking error of the simulation results. Fig. 3(b) shows that the controlled system has a large tracking error with a bound of 0.021 deg at zero velocity. This is a result of the Coulomb friction. When a plant passes by zero velocity, the Coulomb friction changes direction, and the plant has discontinuous nonlinearity. The TDE uses the previous information for **H** at t-L to estimate itself and therefore the TDE error occurs is as large as the changes in the plant dynamics during one sampling time. Therefore, the TDE cannot estimate the hasty change of the Coulomb friction exactly, and the TDE error becomes large at zero velocity, as described in Fig. 3(a). According to such a TDE error and the error dynamics in (11), the controlled system has a large tracking error, as shown in Fig. 3(b).

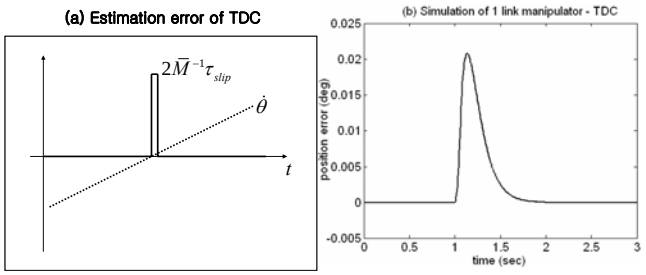

Fig. 3. Effect of the Coulomb friction in the TDC where τ_{slip}=5 Nm and L=0.001 sec.

2.2 Review of the IMC

2.2.1 Structure of the IMC

The IMC, proposed by Garcia and Morari [16], is shown in Fig. 4. It is composed of the IMC controller Q and the internal model G_m. The effect of the parallel path with the model G_m is to subtract the effect of the manipulated variables from the plant output. If it is assumed that the model represents the plant perfectly, then the feedback signal is equal to the influence of the disturbances and is not affected by the actions of the manipulated variables. Thus, the system is effectively an open loop [17].

The IMC controller Q designed based on G_m^{-1} plays the role of a feed-forward controller. But the IMC controller does not suffer from the disadvantages of feed-forward controllers: it can cancel the influence of the disturbances because the feedback signal is equal to this influence and it modifies the controller set point accordingly [17].

The overall transfer function of the IMC is given as:

$$y(s) = \frac{GQ}{1+Q\left(G-G_m\right)}\,y_d + \frac{1-G_mQ}{1+Q\left(G-G_m\right)}\,Gd \;. \qquad (13)$$

The IMC is an intuitive and prominent algorithm. However, there are some limitations to be applied solely to the mechanical field. One limitation is that it requires the plant model, which is very difficult and time consuming to be obtained in complex nonlinear plants, such as robot manipulators. Moreover, the IMC's scheme, in its original design form, results in an open loop control, which is only applicable to stable systems [20]. These are the main reasons why the IMC has been seldom applied to the control of mechanical systems.

2.2.2 Concept of perfect control

Some properties of the IMC can be easily derived from (13) and one is the concept of perfect control [16,20].

- Assume that ① $Q=G_m^{-1}$ is realizable and ② the IMC system is closed loop stable, then the perfect reference tracking control ($y=y_d$) can be achieved from (13) for all t>0 despite any disturbance d.

This indicates perfect reference tracking and complete disturbance rejection. Though perfect control cannot be realized, it is of great theoretical interest. Also, it is a practical issue regarding how closely this ideal can be approached. In the age of digital control, very complex controllers can be implemented with relative ease. Furthermore, if G_m is invertible, it is possible to design a

controller closer to the ideal case, which will work robustly even though the plant has fast dynamics such as Coulomb friction.

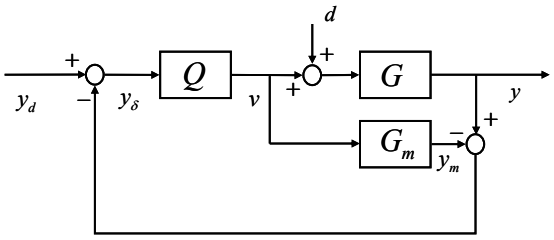

Fig. 4. Block diagram of the IMC where Q denotes the IMC controller, G signifies the plant, and G_m implies the internal model.

3. Time Delay Control with Internal Model(TDCIM)

In this section, an enhanced controller, named the time delay control with internal model (TDCIM), is proposed and its properties are analyzed. Its design procedure is arranged into two steps. In the first step, the closed loop system controlled by the TDC is rearranged into a linear form with the perturbation of the TDE error and in the second step, an additional control loop based on the IMC is designed to compensate for the TDE error.

3.1 Derivation of the TDCIM

3.1.1 Derivation of the linear dynamics from the TDC system

- *Plant linearization using the TDE*

In the TDC, the TDE is used to cancel the nonlinear dynamics of the plant. From (10), the robot dynamics compensated by the TDE can be written as the following linear equation:

$$\ddot{\boldsymbol{\theta}}_{(t)} = \mathbf{u}_{(t)} - \bar{\mathbf{M}}^{-1}\left(\mathbf{H}_{(t)} - \mathbf{H}_{(t-L)}\right) = \mathbf{u}_{(t)} - \boldsymbol{\varepsilon}_{(t)}. \qquad (14)$$

This indicates that the relationship between the joint variable, $\boldsymbol{\theta}$, and control input, $\mathbf{u}$, is described as a linear equation, $\boldsymbol{\theta}=s^{-2}\mathbf{u}$, where the TDE error, $\boldsymbol{\varepsilon}$, can be treated as a disturbance.

- *PD feedback loop*

The control input $\mathbf{u}$ in (5) can be separated as a reference input and feedback input:

$$\mathbf{u} = \mathbf{v} - \left(\mathbf{K}_D\dot{\boldsymbol{\theta}} + \mathbf{K}_P\boldsymbol{\theta}\right), \qquad (15)$$

where $\mathbf{v}$ denotes the reference input: $\mathbf{v} \equiv \ddot{\boldsymbol{\theta}}_d + \mathbf{K}_D\dot{\boldsymbol{\theta}}_d + \mathbf{K}_P\boldsymbol{\theta}_d$. Then, (14) can be rewritten as follows:

$$\ddot{\boldsymbol{\theta}} + \mathbf{K}_D\dot{\boldsymbol{\theta}} + \mathbf{K}_P\boldsymbol{\theta} = \mathbf{v} - \boldsymbol{\varepsilon}. \qquad (16)$$

Finally, the dynamics of $\boldsymbol{\theta}$ can be described as the separate linear dynamics of $\mathbf{v}$, and the TDC system can be simplified as in Fig. 5.

As a result, the TDC system can be explained as a feed-forward controller with the plant linearized by the TDE and PD feedback. Through the linearization process, however, the TDE error occurs and affects the controlled variables as a disturbance.

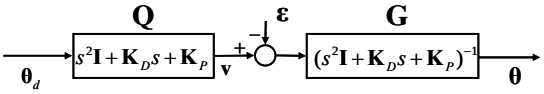

Fig. 5. Simplified block diagram of the TDC with the plant linearized by the TDE and PD feedback.

3.1.2 Compensator design based on the IMC

Now, the compensator based on the IMC is added to the TDC simplified in Fig. 5. According to the design procedure of the IMC [16,17], the internal model $\mathbf{G}_m$ can be easily selected from Fig. 5, as follows:

$$\mathbf{G}_m(s) = \left(s^2\mathbf{I} + \mathbf{K}_Ds + \mathbf{K}_P\right)^{-1}. \qquad (17)$$

Also, the IMC controller can be designed as follows based on the above internal model:

$$\mathbf{Q}(s) = s^2\mathbf{I} + \mathbf{K}_Ds + \mathbf{K}_P.^1 \qquad (18)$$

Fig. 5 shows that the simplified TDC already has a controller such as (18); therefore, the TDCIM can be achieved by adding only an internal model and the IMC feedback, as described in Fig. 6.

Fig. 7 shows the overall block diagram of the TDCIM. In the TDCIM, the combined value of the reference and IMC feedback is used instead of the reference $\boldsymbol{\theta}_d$ of the TDC. The control law of the TDCIM is given as:

$$\boldsymbol{\theta}_{\delta(t)} = \boldsymbol{\theta}_{d(t)} - \boldsymbol{\theta}_{(t-L)} + \boldsymbol{\theta}_{m(t-L)}, \text{ and} \qquad (19)$$

$$\boldsymbol{\tau}_{(t)} = \boldsymbol{\tau}_{(t-L)} - \bar{\mathbf{M}}\ddot{\boldsymbol{\theta}}_{(t-L)} + \bar{\mathbf{M}}\left[\ddot{\boldsymbol{\theta}}_{\delta(t)} + \mathbf{K}_D\left(\dot{\boldsymbol{\theta}}_{\delta(t)} - \dot{\boldsymbol{\theta}}_{(t)}\right) + \mathbf{K}_P\left(\boldsymbol{\theta}_{\delta(t)} - \boldsymbol{\theta}_{(t)}\right)\right] \qquad (20)$$

The TDCIM has a simple structure, as shown in Fig. 9, and does not need extra gain. The control law described above shows that the TDCIM can be designed by choosing only $\bar{\mathbf{M}}$, $\mathbf{K}_D$, and $\mathbf{K}_P$ the same as the TDC case. Furthermore, because of using the TDE, it does not need the entire computation of the robot dynamics. Therefore, it is easily applied and efficient so as to match the positive attributes of the TDC.

- ***Remark 1: time delay due to sampling***

The feedback time delay in the IMC feedback is included in Fig. 7 (dashed box) and (19). It is not included intentionally, but it is inevitable in the discretely implemented controllers. If $\mathbf{Q}=\mathbf{G}_m^{-1}$, the IMC theoretically provides a perfect control scheme, but, it is only possible under a continuous time condition. In many cases, the controllers are designed with a digital platform such as personal computers and work under a discrete time condition. In these cases, it is impossible to prevent a time delay in the feedback due to sampling. Thus, the IMC

[1] The controller needs the velocity and acceleration of the plants. In many cases, however, they are not measured and are thus obtained by numerical differentiations. The numerical differentiations cause a delay in the responses and degrade the tracking performance; however, it is not a critical problem in implementation of a controller. It is also well known that the differentiations enlarge the influence of the sensing noise, but this can be overcome by using a low pass filter [17,21].

cannot work as a perfect controller. So, it is necessary to consider the time delay due to sampling for a more precise analysis.

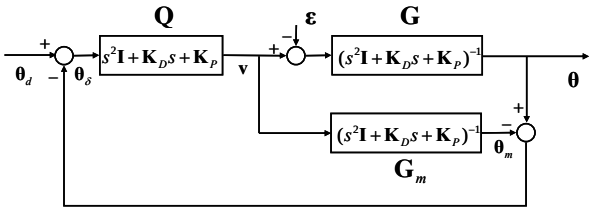

Fig. 6. Simplified block diagram of the TDCIM.

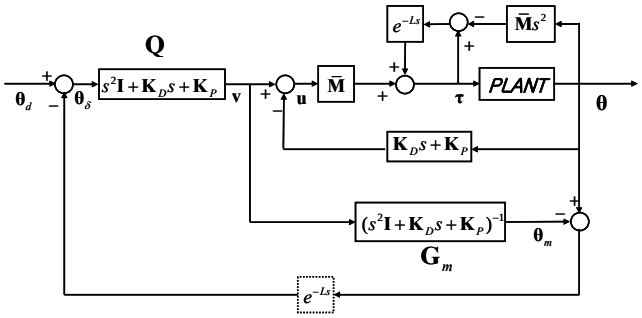

Fig. 7. Overall block diagram of the TDCIM.

3.2 The role of the IMC feedback

To determine the properties of the TDCIM, it is essential to verify the role of the IMC feedback. So, the meaning of the IMC feedback is analyzed.

At first, the control input of the TDC is redefined as follows to prevent confusion with the control input of the TDCIM:

$$\mathbf{u}_{TDC(t)} \equiv \ddot{\boldsymbol{\theta}}_{d(t)} + \mathbf{K}_D \dot{\mathbf{e}}_{(t)} + \mathbf{K}_P \mathbf{e}_{(t)} . \quad (21)$$

Then, the control input of the TDCIM, including the time delay in the IMC feedback, can be described as follows:

$$\begin{aligned}\mathbf{u}_{(t)} = \mathbf{u}_{TDC(t)} - \big[& \ddot{\boldsymbol{\theta}}_{(t-L)} - \ddot{\boldsymbol{\theta}}_{m(t-L)} \\ & + \mathbf{K}_D \left(\dot{\boldsymbol{\theta}}_{(t-L)} - \dot{\boldsymbol{\theta}}_{m(t-L)} \right) + \mathbf{K}_P \left(\boldsymbol{\theta}_{(t-L)} - \boldsymbol{\theta}_{m(t-L)} \right) \big] .\end{aligned} \quad (22)$$

The right side terms, except $\mathbf{u}_{TDC(t)}$, are the additional control inputs from the IMC feedback. Also, their meanings can be obtained by subtracting the plant dynamics **G** in (16) from the internal model dynamics $\mathbf{G}_m$ in (17) at *t-L*:

$$\begin{aligned}\ddot{\boldsymbol{\theta}}_{(t-L)} - \ddot{\boldsymbol{\theta}}_{m(t-L)} + \mathbf{K}_D & \left(\dot{\boldsymbol{\theta}}_{(t-L)} - \dot{\boldsymbol{\theta}}_{m(t-L)} \right) \\ & + \mathbf{K}_P \left(\boldsymbol{\theta}_{(t-L)} - \boldsymbol{\theta}_{m(t-L)} \right) = -\boldsymbol{\varepsilon}_{(t-L)}\end{aligned} . \quad (23)$$

This shows that the IMC feedback value indicates the TDE error before one sampling time. Therefore, the control input and input torque of the TDCIM can be rewritten as:

$$\mathbf{u}_{(t)} = \mathbf{u}_{TDC(t)} + \boldsymbol{\varepsilon}_{(t-L)} , \text{ and} \quad (24)$$

$$\boldsymbol{\tau}_{(t)} = \bar{\mathbf{M}}\mathbf{u}_{(t)} + \hat{\mathbf{H}}_{(t)} = \bar{\mathbf{M}}\mathbf{u}_{TDC(t)} + \mathbf{H}_{(t-L)} + \bar{\mathbf{M}}\boldsymbol{\varepsilon}_{(t-L)} . \quad (25)$$

The TDCIM can be treated as a TDC with a compensator using the TDE error at *t-L*. Also, the error dynamics of the TDCIM is given as follows:

$$\ddot{\mathbf{e}}_{(t)} + \mathbf{K}_D \dot{\mathbf{e}}_{(t)} + \mathbf{K}_P \mathbf{e}_{(t)} = \boldsymbol{\varepsilon}_{(t)} - \boldsymbol{\varepsilon}_{(t-L)} . \quad (26)$$

From another point of view, the TDCIM can be regarded as a controller with an estimator of **H** working as follows:

$$\hat{\mathbf{H}}_{TDCIM(t)} = \mathbf{H}_{(t-L)} + \bar{\mathbf{M}}\boldsymbol{\varepsilon}_{(t-L)} = 2\mathbf{H}_{(t-L)} - \mathbf{H}_{(t-2L)} . \quad (27)$$

This indicates that the compensator decreases the influence of the TDE error and improves the estimation performance of **H** by using the TDE error at *t-L*.

To show the role of the compensator more clearly, it is worthwhile to observe its effect when **H** changes slowly. Fig. 8 shows the estimation values of **H** in the TDC and TDCIM conceptually. The TDC uses the TDE, $\hat{\mathbf{H}}_{(t)} = \mathbf{H}_{(t-L)}$, and the TDE error occurs to the extent of the change in **H** during one sampling time. In the TDCIM, the TDE error is compensated by itself at *t-L*, and thus a more precise estimation is possible. This is an indication that the TDCIM is more robust to the change in **H** than the TDC.

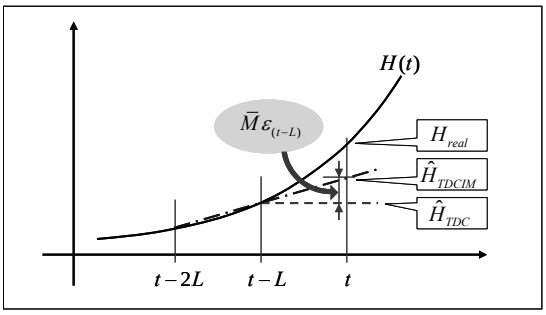

Fig. 8. Estimation of a slow **H** in the TDC and TDCIM.

3.3 Stability analysis of the TDCIM

Sufficient stability conditions have been derived based on an analysis of L_∞^N [22]. The notations used in the stability analysis are presented in Table I.

▪ ***Theorem 1: Stability of the TDCIM***

If the assumption and the stability condition presented below are satisfied, then the robot manipulator controlled by the TDCIM is L_∞ stable.

Assumption: $\mathbf{w}, \boldsymbol{\theta}_d, \dot{\boldsymbol{\theta}}_d, \ddot{\boldsymbol{\theta}}_d \in L_\infty^N$,

Stability condition: $\left\| \mathbf{A}'_{(t)} \right\|_{i2\infty} < 1$ *and* $\left\| \mathbf{B}'_{(t)} \right\|_{i2\infty} < 1$,

where **w** denotes the disturbance and Coulomb or static friction, and the matrices $\mathbf{A}'_{(t)}$, $\mathbf{B}'_{(t)}$ are defined as follows:

▫ *Definition of* $\mathbf{A}'_{(t)}$ *and* $\mathbf{B}'_{(t)}$:

At first, $\boldsymbol{\Lambda}_{(t)} = diag[\lambda_{1(t)}, \cdots, \lambda_{N(t)}]$ and $\mathbf{P}_{(t)}$ is defined as follows to diagonalize $\boldsymbol{\Omega}_{(t)}$:

$$\boldsymbol{\Omega}_{(t)} = \mathbf{P}_{(t)} \boldsymbol{\Lambda}_{(t)} \mathbf{P}_{(t)}^{-1}, \quad (28)$$

where $\boldsymbol{\Omega}_{(t)} = \mathbf{I} - \sqrt{\bar{\mathbf{M}}}\mathbf{M}_{(t)}^{-1}\sqrt{\bar{\mathbf{M}}}$ and $\sqrt{\bar{\mathbf{M}}}$ is defined as the diagonal positive definite matrix that satisfies

$\sqrt{\bar{\mathbf{M}}}\sqrt{\bar{\mathbf{M}}} = \bar{\mathbf{M}}$.

Then $\mathbf{A'}_{(t)}$ and $\mathbf{B'}_{(t)}$ are defined as:

$$\mathbf{A'}_{(t)} = \mathbf{P}_{(t)}^{-1}\mathbf{A}_{(t)}\mathbf{P}_{(t)}, \quad \mathbf{B'}_{(t)} = \mathbf{P}_{(t)}^{-1}\mathbf{B}_{(t)}\mathbf{P}_{(t)}, \tag{29}$$

where $\mathbf{A}_{(t)} = diag[a_{1(t)}, \cdots, a_{N(t)}]$, $a_{i(t)} = \lambda_{i(t)} + \sqrt{\lambda_{i(t)}^2 - \lambda_{i(t)}}$ and $\mathbf{B}_{(t)} = diag[b_{1(t)}, \cdots, b_{N(t)}]$, $b_{i(t)} = \lambda_{i(t)} - \sqrt{\lambda_{i(t)}^2 - \lambda_{i(t)}}$.

▪ ***Proof***

From (19) and (20), the input torque of the TDCIM can be rewritten as:

$$\begin{aligned}\boldsymbol{\tau}_{(t)} &= 2[\boldsymbol{\tau}_{(t-L)} - \bar{\mathbf{M}}\ddot{\boldsymbol{\theta}}_{(t-L)}] - [\boldsymbol{\tau}_{(t-2L)} - \bar{\mathbf{M}}\ddot{\boldsymbol{\theta}}_{(t-2L)}] \\ &\quad + \bar{\mathbf{M}}[\ddot{\boldsymbol{\theta}}_{d(t)} + \mathbf{K}_D\dot{\mathbf{e}}_{(t)} + \mathbf{K}_P\mathbf{e}_{(t)}]\end{aligned}. \tag{30}$$

Also, $\mathbf{F}$ of (1) can be expressed as follows, where $\mathbf{F}_v$ denotes viscous friction and $\mathbf{w}$ is disturbance including the Coulomb and static frictions:

$$\mathbf{F} = \mathbf{F}_v + \mathbf{w}. \tag{31}$$

Then, the error dynamics of the closed loop system can be derived from (1), (30), and (31):

$$\begin{aligned}\tilde{\boldsymbol{\varepsilon}}_{(t)} - 2[\mathbf{I} - \mathbf{M}_{(t)}^{-1}\bar{\mathbf{M}}]\tilde{\boldsymbol{\varepsilon}}_{(t-L)} + [\mathbf{I} - \mathbf{M}_{(t)}^{-1}\bar{\mathbf{M}}]\tilde{\boldsymbol{\varepsilon}}_{(t-2L)}, \\ = \boldsymbol{\psi}_{(t)} + \boldsymbol{\varphi}_{(t)}\end{aligned} \tag{32}$$

where,

$$\begin{aligned}\boldsymbol{\psi}_{(t)} &= [\mathbf{I} - \mathbf{M}_{(t)}^{-1}\bar{\mathbf{M}}][\mathbf{K}_D\dot{\tilde{\mathbf{e}}}_{(t)} + \mathbf{K}_P\tilde{\mathbf{e}}_{(t)}] - \mathbf{M}_{(t)}^{-1}\left[-2\tilde{\mathbf{M}}_{(t)}\ddot{\boldsymbol{\theta}}_{(t-L)}\right. \\ &\quad \left. + \breve{\mathbf{M}}_{(t)}\ddot{\boldsymbol{\theta}}_{(t-2L)} - \tilde{\tilde{\mathbf{V}}}_{(t)} - \tilde{\tilde{\mathbf{G}}}_{(t)} - \tilde{\tilde{\mathbf{F}}}_{v(t)}\right],\end{aligned}$$

and, $\boldsymbol{\varphi}_{(t)} = \mathbf{M}_{(t)}^{-1}\tilde{\tilde{\mathbf{w}}}_{(t)} + [\mathbf{I} - \mathbf{M}_{(t)}^{-1}\bar{\mathbf{M}}]\dddot{\boldsymbol{\theta}}_{d(t)}$.

$\mathbf{e}_{\gamma(t)}$ and $\boldsymbol{\varepsilon}_{\gamma(t)}$ are defined as follows:

$$\mathbf{e}_{\gamma(t)} \triangleq \sqrt{\bar{\mathbf{M}}}\mathbf{e}_{(t)}, \ \boldsymbol{\varepsilon}_{\gamma(t)} \triangleq \sqrt{\bar{\mathbf{M}}}\boldsymbol{\varepsilon}_{(t)}. \tag{33}$$

Then, the following can be derived by transforming (32) into the function of $\mathbf{e}_{\gamma(t)}$ and $\boldsymbol{\varepsilon}_{\gamma(t)}$:

$$\tilde{\boldsymbol{\varepsilon}}_{\gamma(t)} - 2\boldsymbol{\Omega}_{(t)}\tilde{\boldsymbol{\varepsilon}}_{\gamma(t-L)} + \boldsymbol{\Omega}_{(t)}\tilde{\boldsymbol{\varepsilon}}_{\gamma(t-2L)} = \sqrt{\bar{\mathbf{M}}}\boldsymbol{\psi}_{(t)} + \sqrt{\bar{\mathbf{M}}}\boldsymbol{\varphi}_{(t)}. \tag{34}$$

From the definition of $\mathbf{A'}_{(t)}$ and $\mathbf{B'}_{(t)}$ in (29), the relationship $\mathbf{A'}_{(t)} + \mathbf{B'}_{(t)} = 2\boldsymbol{\Omega}_{(t)}$, $\mathbf{A'}_{(t)}\mathbf{B'}_{(t)} = \mathbf{B'}_{(t)}\mathbf{A'}_{(t)} = \boldsymbol{\Omega}_{(t)}$ is valid. So, the above equation is described as follows:

$$\begin{aligned}\tilde{\boldsymbol{\varepsilon}}_{\gamma(t)} - (\mathbf{A'}_{(t)} + \mathbf{B'}_{(t)})\tilde{\boldsymbol{\varepsilon}}_{\gamma(t-L)} + \mathbf{B'}_{(t)}\mathbf{A'}_{(t)}\tilde{\boldsymbol{\varepsilon}}_{\gamma(t-2L)} \\ = \sqrt{\bar{\mathbf{M}}}\boldsymbol{\psi}_{(t)} + \sqrt{\bar{\mathbf{M}}}\boldsymbol{\varphi}_{(t)}\end{aligned}. \tag{35}$$

If $\left\|\mathbf{B'}_{(t)}\right\|_{i2\infty} < 1$ is satisfied, the following can be derived from (35):

$$\begin{aligned}&(1 - \left\|\mathbf{B'}_{(t)}\right\|_{i2\infty})(1 - \left\|\mathbf{A'}_{(t)}\right\|_{i2\infty})\left\|\tilde{\boldsymbol{\varepsilon}}_{\gamma(t)}\right\|_{T\infty} \\ &\le \left\|\sqrt{\bar{\mathbf{M}}}\boldsymbol{\psi}_{(t)} - \mathbf{B'}_{(t)}\tilde{\mathbf{A}}'_{(t)}\tilde{\boldsymbol{\varepsilon}}_{\gamma(t-2L)}\right\|_{T\infty} + \left\|\sqrt{\bar{\mathbf{M}}}\boldsymbol{\varphi}_{(t)}\right\|_{T\infty}\end{aligned} \tag{36}$$

Furthermore, if $\left\|\mathbf{A'}_{(t)}\right\|_{i2\infty} < 1$ is satisfied, the following can be derived from (36):

$$\left\|\tilde{\boldsymbol{\varepsilon}}_{\gamma(t)}\right\|_{T\infty} \le \frac{\left\|\sqrt{\bar{\mathbf{M}}}\boldsymbol{\psi}_{(t)} - \mathbf{B'}_{(t)}\tilde{\mathbf{A}}'_{(t)}\tilde{\boldsymbol{\varepsilon}}_{\gamma(t-2L)}\right\|_{T\infty} + \left\|\sqrt{\bar{\mathbf{M}}}\boldsymbol{\varphi}_{(t)}\right\|_{T\infty}}{(1 - \left\|\mathbf{B'}_{(t)}\right\|_{i2\infty})(1 - \left\|\mathbf{A'}_{(t)}\right\|_{i2\infty})} \tag{37}$$

Letting $T \to \infty$, the following is obtained:

$$\left\|\tilde{\boldsymbol{\varepsilon}}_{\gamma(t)}\right\|_{\infty} \le \frac{\left\|\sqrt{\bar{\mathbf{M}}}\boldsymbol{\psi}_{(t)} - \mathbf{B'}_{(t)}\tilde{\mathbf{A}}'_{(t)}\tilde{\boldsymbol{\varepsilon}}_{\gamma(t-2L)}\right\|_{\infty} + \left\|\sqrt{\bar{\mathbf{M}}}\boldsymbol{\varphi}_{(t)}\right\|_{\infty}}{(1 - \left\|\mathbf{B'}_{(t)}\right\|_{i2\infty})(1 - \left\|\mathbf{A'}_{(t)}\right\|_{i2\infty})}. \tag{38}$$

For a sufficiently small L, $\left\|\sqrt{\bar{\mathbf{M}}}\boldsymbol{\psi}_{(t)} - \mathbf{B'}_{(t)}\tilde{\mathbf{A}}'_{(t)}\tilde{\boldsymbol{\varepsilon}}_{\gamma(t-2L)}\right\|_{\infty}$, which is composed of $\breve{\bullet}$, $\tilde{\tilde{\bullet}}$, and $\breve{\bullet}$, becomes small and its effect can be ignored. Besides, if the assumption is satisfied, $\left\|\sqrt{\bar{\mathbf{M}}}\boldsymbol{\varphi}_{(t)}\right\|_{\infty} < \infty$. Therefore, $\left\|\tilde{\boldsymbol{\varepsilon}}_{\gamma(t)}\right\|_{\infty} \le \infty$, so that $e_{(t)}$ and $\dot{e}_{(t)}$ are bounded. □

As $\bar{\mathbf{M}}$ is similar to $\mathbf{M}_{(t)}$, $\left\|\mathbf{A'}_{(t)}\right\|_{i2\infty}$ and $\left\|\mathbf{B'}_{(t)}\right\|_{i2\infty}$ become smaller, so the TDCIM has a greater possibility to satisfy the stability condition. From the analysis and simulation, it has been detected that the stable gain of the TDCIM is less than that of the TDC.

4. Verification: Simulation and Experiment

4.1 Simulation of the TDCIM under Coulomb friction

The robustness of the TDCIM is verified by simulation, and how the proposed compensator affects the fast dynamics of the system, especially the Coulomb and static frictions, is analyzed. These results are compared with those of the TDC in subsection 2.1.3.

The TDCIM with $\bar{M} = 0.5$ is applied to the 1 DOF manipulator shown in Fig. 2 with the same conditions as in the TDC case. The PD gains are set to K_D=20 and K_P=100 to ensure the error dynamics (26) have natural frequencies of

TABLE I
NOTATIONS

When $\bullet_{(t)}$ is a $N \times 1$ vector	When $\bullet_{(t)}$ is a matrix	When $\bullet_{(t)}$ is a vector or a matrix
$\left\|\bullet_{(t)}\right\| = \sqrt{\bullet_{(t)}^T \bullet_{(t)}}$.	$\left\|\bullet_{(t)}\right\|_{i2}$ is the induced second norm of $\bullet_{(t)}$.	$\tilde{\bullet}_{(t)} = \bullet_{(t)} - \bullet_{(t-L)}$.
$\left\|\bullet_{(t+c)}\right\|_{\infty} = \sup_{t \ge 0}\left\|\bullet_{(t+c)}\right\|$ (This means L_{∞}^{N})		$\tilde{\tilde{\bullet}}_{(t)} = \tilde{\bullet}_{(t)} - \tilde{\bullet}_{(t-L)}$.
$\left\|\bullet_{(t+c)}\right\|_{T\infty} = \sup_{0 \le t \le T}\left\|\bullet_{(t+c)}\right\|$.	$\left\|\bullet_{(t)}\right\|_{i2\infty} = \left\|\left\|\bullet_{(t)}\right\|_{i2}\right\|_{\infty}$.	$\breve{\bullet}_{(t)} = \bullet_{(t)} - \bullet_{(t-2L)}$.
		(where L denotes the sampling time)

ω_n=10 rad/sec with critical damping.

The simulation results of the TDCIM against Coulomb friction are shown in Fig. 9: (a) is the conceptual figure of the estimation errors of **H** in the TDCIM and (b) is the tracking error of the simulation results. Fig. 9(b) shows that the tracking error of the TDCIM has an error bound of 0.001 deg. This error bound is dramatically reduced compared with the result of the TDC, and represents robustness of TDCIM against discontinuous dynamics such as Coulomb friction. Furthermore, it can be explained from the estimation error of **H**. After the TDE error occurs due to the Coulomb friction effect, a counter action appears from the compensation using $\boldsymbol{\varepsilon}_{(t-L)}$, as described in Fig. 9(a); furthermore, it eliminates the influence of the TDE error and considerably reduces the tracking error as shown in Fig. 9(b).

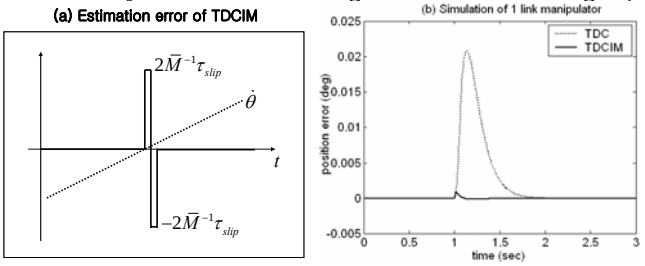

Fig. 9. Effect of the Coulomb friction in the TDCIM where τ_{slip}=5 Nm and L=0.001 sec.

4.2 Experiment

In this subsection, the robustness of the TDCIM is verified by the experimental results of a 2 DOF planar robot and is compared with that of the TDC. The planar robot used in the experiments is shown in Fig. 10 and its specifications are provided in Table II.

4.2.1 Experimental set up

Fig. 11 shows the reference trajectory that makes the end effecter draw a circle with a 10 mm radius during 4 seconds. Both the sampling time and the time delay for the TDE are set to L=0.001 sec.

$\bar{M} = diag(\alpha_1, \alpha_2)$ of the TDC and TDCIM described in Table III are tuned to minimize the tracking error. The PD gains are set to k_{Di}=20 and k_{Pi}=100 for both controllers to make natural frequencies of ω_n=10 rad/sec and damping ratios ζ=1 of the error dynamics (11) and (25), where i denotes the joint number.

Fig. 10. 2 DOF planar robot system

TABLE II
SPECIFICATIONS OF THE 2 DOF PLANAR ROBOT

	Link 1	Link 2
Length (m)	0.35	0.29
Mass (kg)	11.17	6.82
Mass center from joint axis (m)	0.30	0.18
Stall torque (Nm)	2.39	0.92
Gear ratio	80:1	100:1

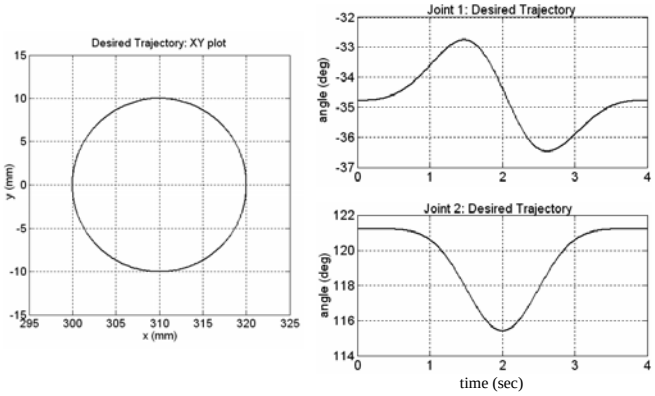

Fig. 11. Desired trajectory

TABLE III
CONTROL GAINS ($\bar{M} = diag(\alpha_1, \alpha_2)$) FOR SCARA ROBOT

	TDC	TDCIM
α_1	0.1	0.03
α_2	0.025	0.0058

4.2.2 Experimental results

The experimental results are arranged in Figs. 12 and 13. Fig. 12 represents the tracking error and torque of each joint and Fig. 13 shows the XY position responses of the end effecter. The maximum tracking errors are presented in Table IV. From the results in Fig.12(a) and (c) compared with the references in Fig. 11, it can observed that the plant controlled by the TDC has a large tracking error due to Coulomb friction when the plant passes by zero velocity. In the TDCIM case, the tracking error is reduced dramatically and confirms that the compensator works well. Fig. 12(b) and (d) show that the TDCIM has a similar torque profile to that of the TDC and does not increase unwanted effects such as chattering. This desirable result shows that the TDCIM has little adverse effect due to the addition of the IMC feedback.

Through the above experimental results, it is verified that the TDCIM is applicable to a multi DOF system and improves the robustness of the TDC against discontinuous friction.

5. Conclusion

This paper reveals the robustness problem of the TDC associated with the TDE error in the tracking control of robot manipulators under discontinuous dynamics, especially the Coulomb frictions. To control and manage the effect of the TDE error, an enhanced controller is proposed using a compensator designed based on the IMC concept,

and the proposed controller's properties and stability conditions are analyzed. Through the simulation of a 1 DOF link system and experiments with a 2 DOF planar robot, the proposed controller's robustness is verified when the TDE error becomes large due to discontinuous friction.

The advantages of the proposed controller can be arranged into two areas: effectiveness and efficiency. The compensator using the IMC can compensate for the effect of the TDE error accurately and improve its robustness against fast friction dynamics. In addition, the proposed compensator also has a simple structure to match the positive attributes of the TDC. Furthermore, it does not need extra tuning of gain or additional hardware: the inclusion of several lines of program code is enough. Therefore, it can be easily applied.

Acknowlodgement

This work was supported by the SRC/ERC program of MOST/KOSEF (grant #R11-1999-008).

6. References

[1] K. Youcef-Toumi and Osamu Ito, "A Time Delay Controller for Systems with Unknown Dynamics," *Trans. of ASME, J. Dyn. Sys., Meas., Contr.*, vol. 112, no. 1, pp. 133-142, 1990.

[2] T. C. Hsia and L. S. Gao, "Robot Manipulator Control Using Decentralized Linear Time-Invariant Time-Delayed Joint Controllers," *IEEE Int. Conf. on Robotics and Automations*, pp. 2070-2075, 1990.

[3] T. C. Hsia, T. A. Lasky, and Z. Guo, "Robust Independent Joint Controller Design for Industrial Robot Manipulators," *IEEE Transactions on Industrial Electronics*, vol. 38, pp. 21-25, 1991.

[4] R. C. Bonitz and T. C. Hsia, "Internal force-based impedance control for cooperating manipulators," *IEEE Trans. Robotics and Automation*, vol. 12, pp. 78-89, 1996.

[5] S. Jung, T. C. Hsia, and R. G. Bonitz, "Force tracking impedance control of robot manipulators under unknown environment," *IEEE Transactions on Control Systems Technology*, vol. 12, pp. 474-483, 2004.

[6] P. H. Chang, D. S. Kim, and K. C. Park, "Robust force/position control of a robot manipulator using time-delay control," *Control Engineering Practice*, vol. 3, pp. 1255-1264, 1995.

[7] P. H. Chang, Byung S. Park, and Ki C. Park, "An experimental study on improving hybrid position/force control of a robot using time delay control," *Mechatronics*, vol. 6, pp. 915-931, 1996.

[8] Pyung Hun Chang and Soo-Jin Lee, "A straight-line motion tracking control of hydraulic excavator system," *Mechatronics*, vol.12, iss.1, pp.119-138, 2002.

[9] J. Y. Park and P. H. Chang, "Vibration control of a telescopic handler u sing time delay control and commandless input shaping technique," *Co ntrol Engineering Practice*, vol. 12, iss. 6, pp. 769-780, 2004.

[10] B. Armstrong, "Friction: experimental determination, modeling and compensation," in *Proc. IEEE Int. Conf. Robotics and Automation*, vol. 3, pp. 1422-1427, 1988.

[11] M. Kermani, M. Wong, R. Patel, M. Moallem, and M. Ostojic, "Friction Compensation in low and high-reversal-velocity manipulators," *IEEE Int. Conf. Robotics and Automation*, vol. 5, pp. 4320-4325, 2004.

[12] Sung-Uk Lee and Pyung Hun Chang, "Control of Heavy-duty Robotic Excavator Using Time Delay Control with Integral Sliding Surface," *Control Engineering Practice,* vol. 10, iss. 7, pp. 697-711, 2001.

[13] Pyung Hun Chang and Suk Ho Park, "On improving time-delay control under certain hard nonlinearities," *Mechatronics*, vol. 13, iss. 4, pp. 393-412, 2003.

[14] J. H. Park and Y. M. Kim, "Time-Delay Sliding Mode Control for a Servo," *Trans. Of ASME, J. Dyn., Sys., Meas., Contr.*, vol. 121, pp. 143-148, 1999.

[15] S. J. Kwon and W. K. Chung, "Robust Performance of the Multiloop Perturbation Compensator," *IEEE/ASME Trans. Mechatronics*, vol. 7, no. 2, June 2002.

[16] C. E. Garcia and M. Morari, "Internal Model Control. 1. A Unifying Review and Some New Results," *Ind. Eng. Chem. Process Des. Dev.,* vol. 21, no. 2, pp. 308-323, 1982.

[17] M. Morari and E. Zafiriou, *Robust Process Control*, Prentice Hall, Englewood Cliffs, NJ, 1989.

[18] S. F. Graebe, M. M. Seron, and G. C Goodwin, "Nonlinear tracking and input disturbance rejection with application to pH control," *J. Proc. Cont.*, vol. 6, no. 2/3, pp. 195-202, 1996.

[19] Q. Hu, P. Saha, and G. P. Rangaiah, "Experimental evaluation of an augmented IMC for nonlinear systems," *Control Engineering Practice*, vol. 8, pp. 1167-1176, 2000.

[20] Q. Li, A. N. Poo, and C. M. Lim, "Internal Model Structure in the Control of Robot Manipulators," *Mechatronics*, vol. 6, no. 5, pp. 571-590, 1996.

[21] K. Youcef-Toumi and S. T. Wu, "Input/Output Linearization Using Time Delay Control," *Trans. Of ASME, J. Dyn., Sys., Meas., Contr.,* vol. 114, pp.10-19, 1992.

[22] Sang Hoon Kang, Maolin Jin, Pyung H. Chang, and Eunjeong Lee, "Nonlinear Bang-Bang Impact Control for Free Space, Impact and Constrained Motion: Multi-DOF Case," *American Control Conference*, Oregon, USA, June 2005.

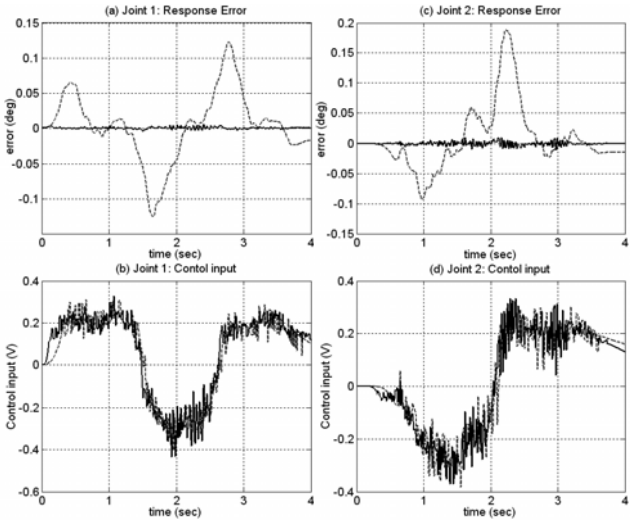

Fig. 12. Experimental results (solid: TDCIM; dashed: TDC).

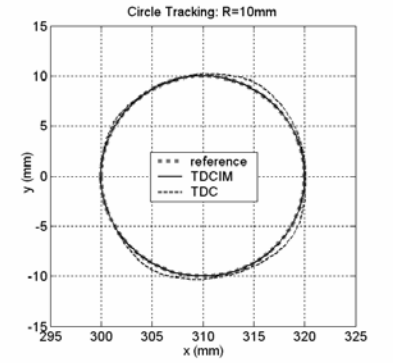

Fig. 13. Experimental results – XY plot.

TABLE IV
MAXIMUM TRACKING ERRORS IN THE TDC AND TDCIM

Symbol	① TDC	② TDCIM	②/①*100
Joint 1	0.1257 deg	0.0049 deg	3.9%
Joint 2	0.1883 deg	0.0107 deg	5.7%